JOURNAL OF MATERIALS SCIENCE 19 (1984) 895–914

Pores as fracture origins in ceramics

ROY W. RICE
Naval Research Laboratory, Washington, DC 20375, USA

Experimental studies and analysis of literature data show that while refinements are needed in fracture mechanics models of pores as flaws in glasses, such models are in reasonable overall agreement with observed strength behaviour. Thus, in glasses, single pores are generally "blunter" flaws than machining or other cracks. However, in polycrystalline materials single pores generally act as sharp cracks. Reasons for this glass–polycrystalline difference in terms of mechanisms and their relation to the models are discussed, along with differences in predicted and observed fracture paths. Quite variable and complex behaviour is indicated for origins from two or more pores in glass and polycrystalline bodies.

1. Introduction

A major change in the concepts of how pores effect tensile strengths of ceramics has occurred in recent years, e.g. as reviewed by Rice [1]. Briefly, strength reductions from porosity were previously viewed as resulting from stress concentration effects of pores increasing the stress on nearby flaws. Pores themselves were not considered as flaws or an integral part of flaws, apparently because they were "so blunt".

More recently, Evans, Davidge and colleagues [2–5] suggested that pores in polycrystalline materials would form equatorial cracks approximately one-half grain deep into the matrix and thus become sharp flaws. The rationale was that grain boundaries intersecting the pore were weak enough to fail, owing to the stress concentration of the pore, so a crack would propagate into the matrix, along grain boundaries, until it encountered the next set of grains (actually approximately one-half grain deep; Fig. 1). Thus, the pore radius, R, plus $L_1 \sim G/2$ was taken as the size of an equivalent sharp flaw in the Griffith equation. Bowie's solution [6] for an infinite cylindrical hole with one or two cracks in a single axial plane (Fig. 1) was subsequently applied [5] as an approximation to the closed, typically more nearly spherically shaped pores in polycrystalline bodies. This solution gives a "correction factor" that provides a transition from a "pure" pore, or "blunter" flaw, to a one-to-one equivalence between the pore + crack and a sharp flaw (Fig. 2). Closely spaced pores, e.g. with centre-to-centre separation of $< 4R$, were suggested to link together to form a flaw whose size was the cluster envelope [5].

Experimentally, the concept of pores as sources of failure has been extensively verified [1, 7, 8], but two discrepancies from the above flaw model have been found [1, 8]. First, a one-to-one equivalence with sharp flaws has been indicated over a much broader range of pore-size to grain-size ratios than had been predicted using Bowie's theory as an approximation. Second, contrary to the original concept of intergranular failure of the first layer of grains around the pore, extensive to total transgranular failure is often found.

Recently, Baratta [9–11] presented a fracture-mechanics model specifically for stress intensities of internal spherical or hemispherical (surface) pores with equatoral cracks. Evans [12] and Green [13] have also since modelled internal pores, thus replacing Bowie's cylindrical-hole model as an approximation for most pores. From these spherical-pore models one can obtain a correction factor, σ_p/σ_a, relating the failure stress, σ_p, from a pore plus an equatorial flaw to the failure stress, σ_a, from a sharp flaw of the same net diameter as the pore plus the equatorial crack. This correction factor is similar to but lower than that from Bowie's model (Fig. 2), so previous discrepancies from using Bowie's model apply to

0022–2461/84 $03.00 + .12

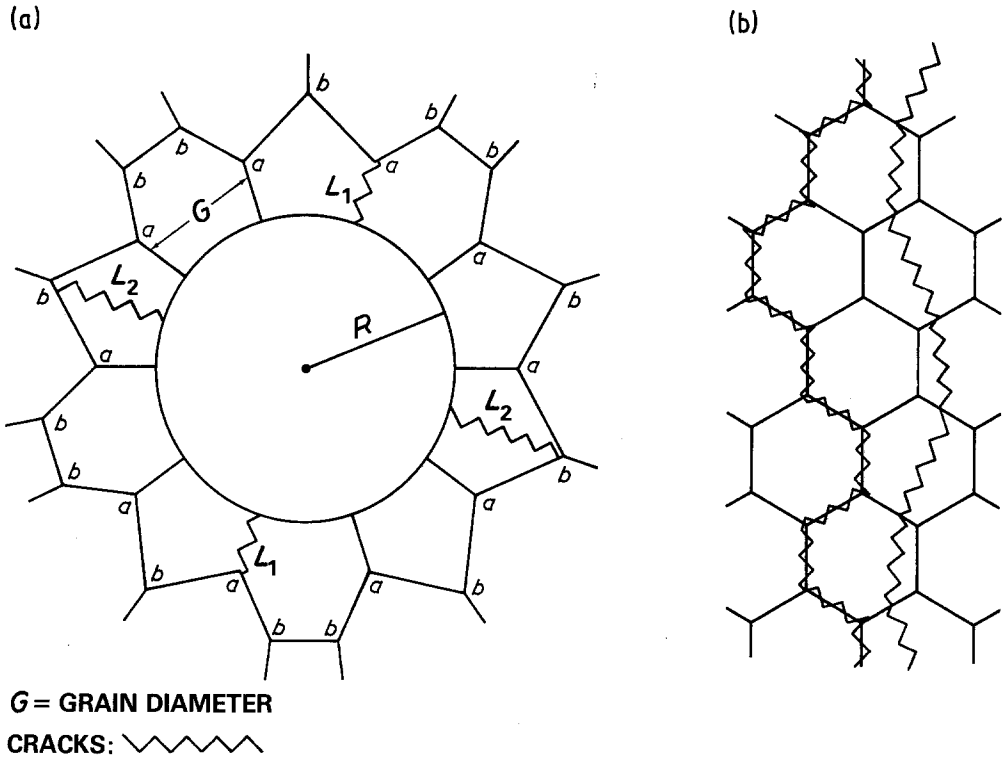

Figure 1 Schematic representation of how grains around a pore in a polycrystalline body interact with the pore to form a pore–flaw combination. (a) Cross-section of the pore. The original proposal was that an equatorial crack, L_1, would propagate from the surface of the pore along grain boundaries because of their weakness until it met the next layer of grains, i.e. at triple points of type **a**, where it would arrest because greater energy would be required to go round or through the second layer of grains. Therefore, the flaw size could be taken as the radius of the pore R, plus the depth of the crack $L_1 = \sim G/2$. An alternative possibility presented in this paper is that cracks of depth $L_2 \sim G$ form transgranularly, arresting at the deeper set of triple points of type **b**. (b) Section of the pore wall mapped onto a plane schematically showing inter- and transgranular cracks.

the spherical-pore models as well. Therefore, the purpose of this paper is to study experimentally the applicability of, and deviations from, these models. Both glass and polycrystalline materials were studied. Bubbles in glass allow testing of the model in the absence of microstructure.* The focus will be on single, isolated pores, but observations on pore clusters will also be made.

2. Experimental procedure

Plates of a germanate† and a laboratory silicate glass, found to contain approximately spherical pores (bubbles) of various sizes and spatial distributions, were utilized. Bars, whose size depended on the size and depth of the pores below the surface, were cut with thickness-to-width ratios in the range 1:1 to 1:2, and lengths so that ratios of flexure span to thickness would typically be $\gtrsim 5$. The tensile surfaces of the bars were either as-cast (airside), or ground parallel to the tensile axis, as in other studies [14]. In either case the edges of the bars were rounded. Additionally, some similar bars of flame-polished soda–lime glass‡ were used, since bubbles were often found in the flame-polished surface, especially when the surface had been ground prior to flame polishing.

Lead zirconate titanate bars, many with purposely introduced spherical pores (diameter $\leqslant 100\ \mu m$) from another study [15–17] were obtained.§ Strengths of the specific bars as tested in that study were used, then the remaining pieces were cut lengthwise into narrower bars

*Because of questions of the effect of microstructure Baratta restricted application of his model to cases where the pore was very large in comparison to the grain size. He also restricted the application to cases where internal pores were no closer than four diameters to the surface and where no other defect was within four diameters of the pore.
†9754 from Corning Glass, Corning, New York, USA.
‡Lustraglass double strength, American St Gobain Corp., Kingsport, Tennessee, USA.
§Courtesy of D. R. Biswas, then of the University of California, Berkeley, California, USA.

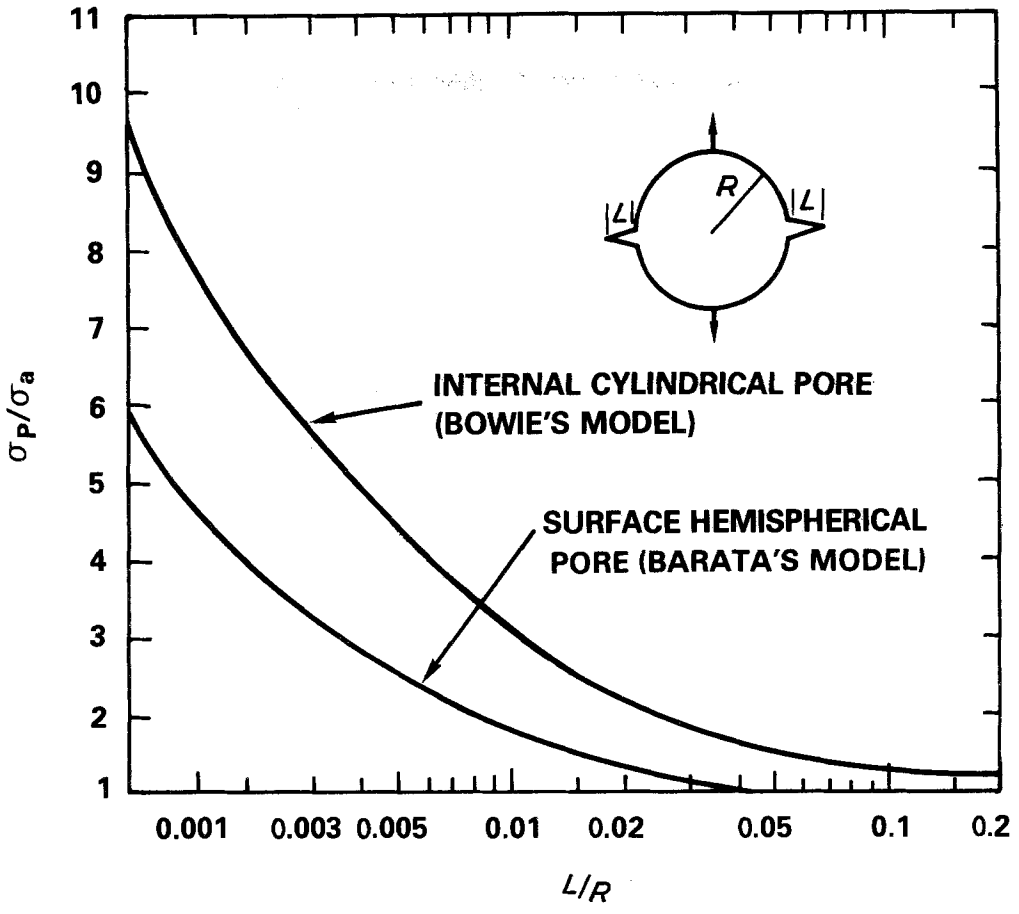

Figure 2 Filure stresses from pores as a function of the ratio of the size of the equatorial crack, L, and the pore radius, R. Note that the stress for failure from the pore, σ_p, is normalized by the failure stress, σ_a, from a sharp flaw of size $R + L$. The curve for a surface void from Baratta's model for a surface pore is shown along with the curve from Bowie's cylindrical-pore flaw model (with a crack on both sides of the pore). The curve for an interior spherical pore would be between these two curves. Although the present models yield σ_p, and hence $\sigma_p/\sigma_a \to \infty$ as $L \to 0$, which is not valid, values of $\sigma_p/\sigma_a \leqslant \sim 5$, i.e. $L/R > \sim 0.002$, should be valid.

(typical cross sections 1.27 x 3.45 mm), had their edges rounded, and were tested on a span of 1.27 cm.

All bars were tested in air at ~ 22° C, ~ 40% rh (relative humidity), in three-point flexure at a crosshead speed of 1.27 mm min^{-1}. Fracture origins, mirrors, and other pertinent fractographic features were determined by standard techniques [18] using optical and scanning electron microscopy. The ratio of the fracture mirror radius (M)* to the radius of the failure-causing flaw, pore, to pore + flaw combination was determined† and compared with the typical values (~ 14 ± 3) for similar dense glasses [19, 20]. Additional data for analysis was obtained from Mecholsky [21] on bulk SiO_2-based glass rods (with flame-polished surfaces), and on SiO_2-based optical fibres [22] along with polycrystalline data from previous studies of the author [1, 7, 8, 23], as well as work on Co-bonded WC [24].

Fracture energies were calculated from strengths and flaw sizes (from fracture examinations), using

$$\sigma = Z\left(\frac{E\gamma}{a}\right)^{1/2} \quad (1)$$

where σ is the failure stress, E is Young's modulus (typical literature values), γ is the fracture surface

*Measured along the tensile surface, but compensating for any surface variations; i.e. extrapolating a smooth mirror boundary to the surface where irregularities or deviations can occur in the mirror boundary.

†All such ratios are designated as M/a.

energy, a is the flaw size and Z is a parameter dependent on flaw shape and location obtained from Irwin and Paris [25], e.g. $Z = 1.12$ for a surface half-penny flaw and 1.25 for an internal penny flaw. For origins associated with pores in glasses the a values were taken as follows: (a) single internal pores: $a = R$, since the size of associated cracks generally could not be accurately determined; (b) individual pores at, or open to, the tensile surface: a was taken as the appropriate radius either of the best-fitting semiellipse or of a surface half-penny (i.e. semicircular) flaw of the same cross-sectional area as the pore when substantially more or less than half of the pore was left at the surface (no clear differences were seen between these two approaches); (c) two or more poles: values of a were taken as the appropriate radii of (i) the best-fitting elliptical envelope of all or part of the pore group (e.g. depending on variable pore spacing), (ii) a circular flaw of the equivalent cross-sectional area of the pores (based on the observation that irregular flaws can be treated as a circular or semicircular (surface) flaw of equal area [26], or (iii) larger individual pores as discussed later. For pore origins in polycrystals, a was taken as R as for the comparable glass cases above plus $G/2$, except as noted otherwise.

Fracture energies calculated using the above a (and corresponding Z) values for failure from pores are designated γ_p, i.e. neglecting any σ_p/σ_a corrections. For those cases where failure occurred from only a sharp surface (e.g. machining) flaw, a and Z were determined from the best visual approximation of them by a semiellipse. These, as well as literature values of fracture energies, i.e. those measured with a sharp flaw, are designated γ_a.

The ratio of the stress for failure from pores against that for failure from sharp flaws of the same size (σ_p/σ_a) for glasses was calculated as follows. (a) For those samples failing from pores: σ_p was taken as the failure stress and σ_a as the stress to cause failure from a sharp flaw of the same size, which is the same as taking the square root of the ratio of the apparent fracture-energy, γ_p, calculated from the failure stress using the pore dimensions as the dimensions of a sharp flaw, to the known fracture-energy, γ_a. (b) For those cases in which failure was from a flaw and not a nearby pore: a lower bound on σ_p/σ_a was obtained by calculating the square root of the ratio γ_p/γ_a as in (a). For polycrystalline specimens, a first approximation of σ_p/σ_a was obtained from the curve of Baratta (Fig. 2) using $G/2$ as the size, L, of the crack emanating from the pore. Other values of L were evaluated in some cases, as discussed later.

3. Results and discussion

3.1. Glass specimens

3.1.1. Strength and fracture initiation

Strengths varied depending on surface finish, bubble size, etc. (Table I, Figs. 3 to 12). Glass samples often did not fail from individual pores (bubbles) intersecting the tensile surface (e.g. Figs. 3 and 4), or somewhat below the tensile surface (Fig. 5), but instead failed from nearby, smaller flaws (e.g. Figs. 4 and 5). This clearly shows that single pores in glasses are often not equivalent to sharp flaws in glasses, which is qualitatively consistent with the models of Baratta, Evans and Green.

Some specimens however failed from single pores intersecting the tensile surface (e.g. Figs. 6 to 9), and one specimen failed from an internal pore* (e.g. Fig. 10). A few cases of failure from two or more bubbles near, or intersecting, the tensile surface were found (Figs. 11 to 13, Table I). In contrast with the case for single pores, no cases of failure from nearby flaws were found when groups of pores were available for fracture. Thus pores, and pore groups, can clearly act as flaws in glasses, the latter being the more serious sources of failure.

3.1.2. Detailed fractography and analysis of single-pore origins

Four fractrographic observations pertinent to more detailed analysis are as follows. (a) Fracture tails frequently extended from the pores (e.g. Figs. 8 and 10), always on the side of the pore having the shorter distance from pore to mirror boundary. Only one case (Fig. 7) was found with neither a fracture tail nor significant mirror asymmetry. (b) Fracture mirrors were often highly asymmetric (e.g. Figs. 6, 8 and 9 with the most and the least anisotropy being observed when no fracture tails were present). (c) For pores adjacent to or intersecting the tensile surface, chips or cracks often extended along the

*Such internal failure typically occurred from high quality, e.g. flame polished, surfaces – see Fig. 8.

TABLE I Data for fracture from pores in glasses

Glass*	SC†	Fracture stress ‡σ_f		Pore§		Flaw size, a (μm)¶			Mirror** radius, R_m (μm)	γ_p (J m^{-2})¶,††			σ_p/σ_a¶,‡‡			M/a¶			$(\sigma_p/\sigma_a)^2 (M/a)$§§		
		(MPa)	(10^3 psi)	No., loc.	R (μm)	A	B	C		A	B	C	A	B	C	A	B	C	A	B	C
1. Single-pore origins																					
	FP	113	16.3	1, S	43			61	550, 350			9.1			1.5			9.0			20
Soda–lime (7)	FP	104	15.1	1, S	35			48	350			6.1			1.2			7.3			11
(12)	FP	81	11.7	1, S	100			110	950, 500			8.4			1.4			8.0			17
	G	50	7.27	1, I	1000			1000	–			5.9			1.2			–			–
		(25)	(3.64)																		
(13)	G	53	7.65	1, S	400			550	1500, 390			18			2.1			2.7			12
Laboratory¶¶	G	128	18.5	1, S	140			140	440, 190			27			2.6			3.1			21
SiO_2 fibre	as drawn	1100	160	1, S	1				8			32			2.8			6			47
SiO_2	FP	360	52	1, S	7.5			11	135, 115			17			2.1			12			53
SiO_2 (8)	FP	520	76	1, I	5.5			5.5	100, 80			8.8			1.5			18(14)			40(32)
		(410)	(60)																		
2. Failure with two or more pores at or near the origins																					
Laboratory	G	105	15.3	2, S	210, 36	180	172	170	1700, 210	24	23	22	2.4	2.4	2.3	9.4	9.9	10	54	57	53
SiO_2	FP	510	74.0	2, S	8, 4	14	13	11	50	43	40	34	3.3	3.1	2.9	3.6	3.9	4.5	39	37	38
								6				18						8.3			
Laboratory (11)	G	92	13.3	3, S	20–40	47	36	14–28	250	4.6	3.6	1.4–2.8	1.0	–	–	5.3			5.3		
Soda–lime	FP	124	18.0	5, S	~10	49	32	4	260	8.9	5.8	2.5	1.5	1.2	–	5.3	8.1		12	12	–
SiO_2 (11)	FP	654	94.9	10, S	2–5	25	~20	3–7	40	126	101	15–35	5.5	5.0	1.9–2.8	1.6	~2.0	13–5.7	48	50	68–44

*Numbers in parentheses refer to figure numbers in which a fracture is shown.

†SC = surface condition; FP = flame polished; G = ground parallel to the tensile axis.

‡⩽ indicates tests on round rods, and the fact that the origin may not be on the vertical axis, so the stress is approximately the value shown, as are all resultant calculated values dependent on σ_f; figures in parentheses give the stress corrected to the centre of internal voids.

§No. = number; loc. = location; I = internal; S = surface; R = radius.

¶For case A, a is the envelope of the pore cluster; for B, a is the radius of a semiciruclar flaw of the same area as the cross-sectional area of the pores in the cluster exposed on the suface; and for C, a is the radius of the pore if it is internal, or half-exposed at the surface, otherwise it is the radius of a semicircular falw of equivalent cross-sectional area to the exposed cross-section of the pore. For case C most a values are larger than the pore radius since more than half the pore was left at the surface.

**Measured parallel with the tensile surface, i.e. at constant stress, for rectangular bars. For round rods failing from the surface, the measurement was parallel with the tangent at the origin. For internal origins, the two extreme values, regardless of direction, are given since it is not known whether such failures occurred on the vertical axis of the specimen or not.

††γ_p = the fracture energy calculated from the Griffith equation assuming the pore or pore group is the flaw.

‡‡$\sigma_p/\sigma_a = (\gamma_p/\gamma_a)^{1/2} = \frac{1}{2}\gamma_p$ (since $\gamma_a \sim 4$), as discussed in the text. Note that values are typically an upper limit, as discussed in the text.

§§Note that the values shown can be much higher than the true value, owing to decreases of σ_p/σ_a and M/a for possible larger values of a, as noted in the text.

¶¶See Fig. 15, reference 22.

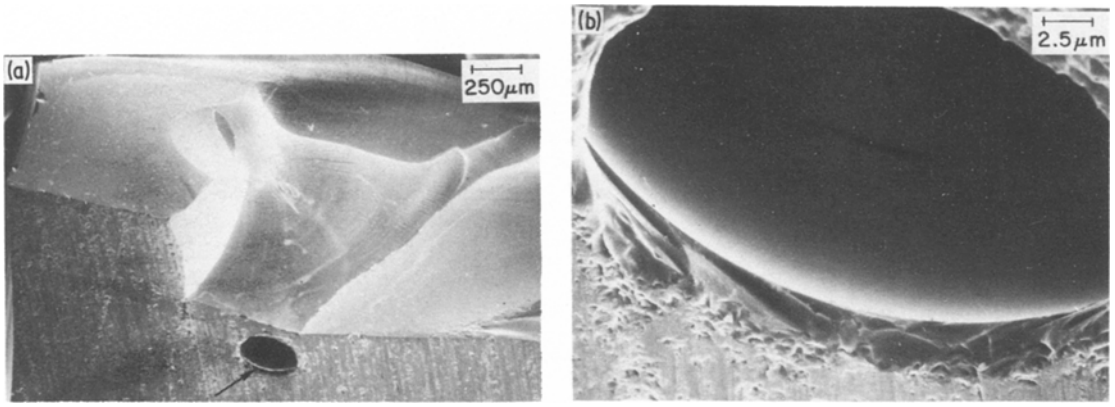

Figure 3 Fracture of a soda–lime glass specimen near, but not from, a large pore exposed at the surface (arrow in (a)). (b) Higher-magnification examination of the intersection of the pore and the surface (ground parallel with the tensile axis) showed some chipping but no obvious cracks associated with the pore. The failure stress of 7.64×10^3 psi (53 MPa) gives $\sigma_p/\sigma_a > 1.1$.

subsequent fracture surface from one or both intersections of the pore with the tensile and fracture surfaces (e.g. Figs. 6 and 9). Such chips or cracks were seen only with fracture tails or highly asymmetric mirrors. (d) Wallner and related lines sometimes outlined the crack-front positions (e.g. Figs. 8 and 9).

These fracture observations show the following fracture sequence and mechanisms. Fracture tails represent the typical overlap and joining of

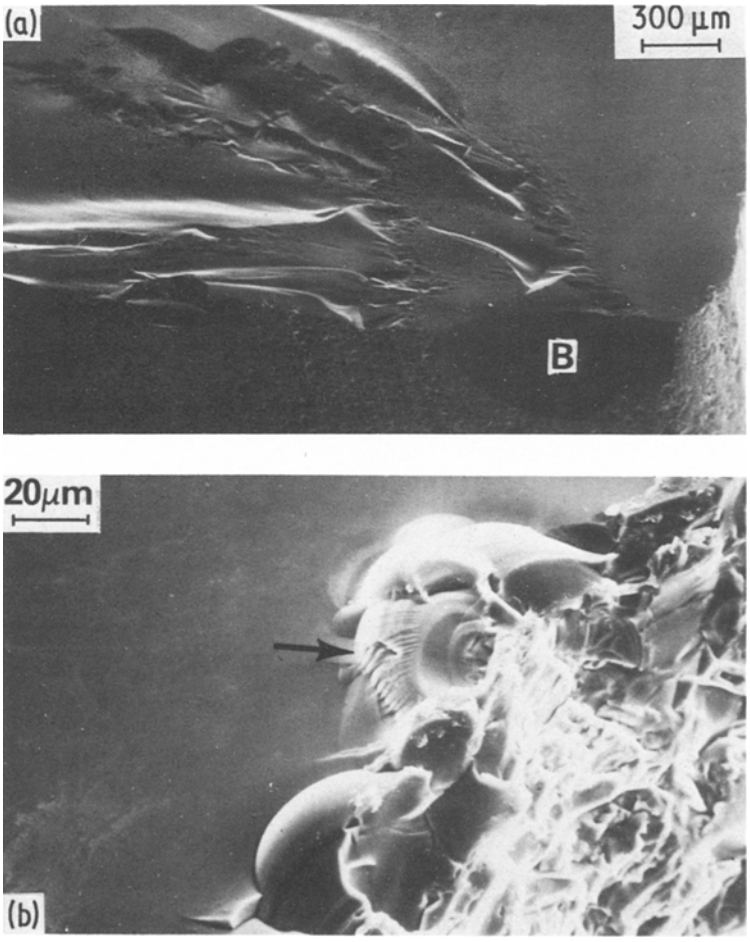

Figure 4 Failure of a germanate glass specimen from a flaw near the remainder of a large pore exposed by machining. The specimen failed from a flaw on the rounded edge shown in the lower right hand corner of the photo to the right of the pore, B. The failure-initiating flaw (arrow in (b) and the failure stress of 13.8×10^3 psi (95 MPa) give $\gamma_a \sim 5\,J\,m^{-2}$. Treating the pore as a semi-elliptical flaw gives a $\sigma_p/\sigma_a > 3.3$. Note that the ratio of mirror size to flaw size of approximately 15 is well within the range of typical values found for most glasses.

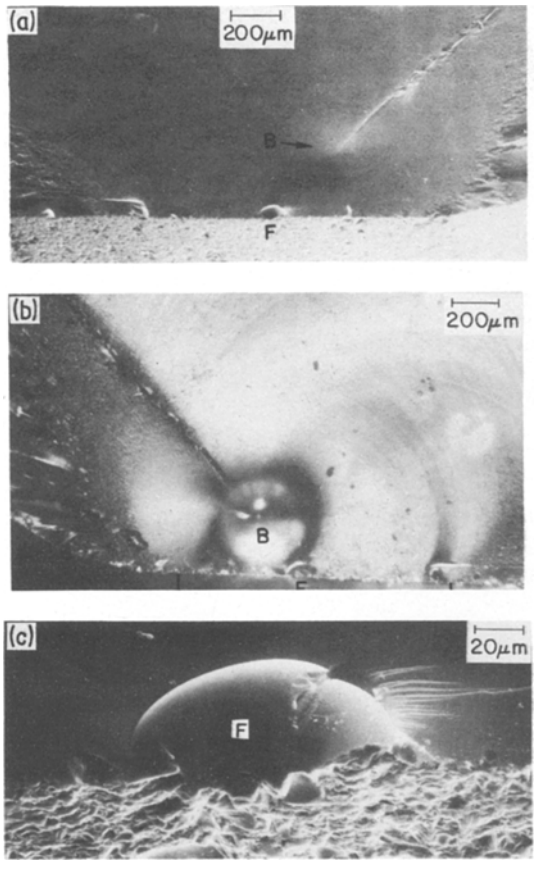

Figure 5 Failure of a soda–lime glass specimen from a flaw near a void. (a) SEM photograph of much of the fracture showing the flaw, (F, from which failure initiated) and the slight hump where the fracture surface is bowed out over the pore (bubble) B, underneath, and the resultant trail of mistlike character extending toward the upper right hand corner. (b) Optical photomicrograph of this same fracture, using side lighting to show the bubble B just below the surface and its proximity to the failure-initiating flaw, F, just to the right of the lower edge of the bubble. (The reversal between (a) and (b) is due to the inversion in the optical microscope.) (c) shows more of F which with the failure stress of 11.8×10^3 psi (81 MPa) gives $\gamma_a \sim 4\,J\,m^{-2}$. M/a on either side of the mirror is ~ 10, i.e. somewhat low but within the range typically found for glasses and hence consistent with failure from the sharp flaw. Treating the bubble as a flaw (and using the stress corrected to the centre of the void of 10.2×10^3 psi (70 MPa)) gives $\sigma_p/\sigma_a > 1.7$.

two cracks not quite on the same plane [18]. The fracture tail from the internal-pore origin is thus consistent with failure starting from part of the pore surface, then spreading in both directions around the pore and overlapping when they meet upon enveloping the pore. On the other hand, fracture tails from pores intersecting the tensile surface show that failure started at two different

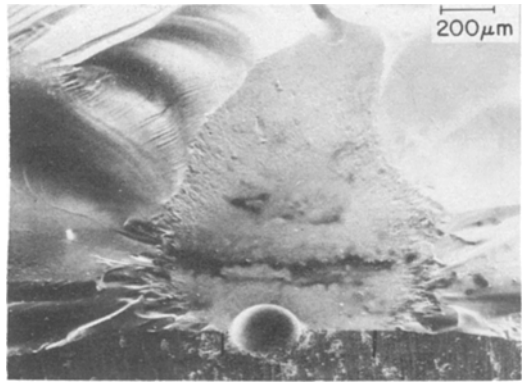

Figure 6 Example of a failure in a laboratory silicate glass from a large void exposed at the surface by grinding (parallel with the tensile axis of the bar). Note the high asymmetry of the mirror. Examination at higher magnification shows that there is some chipping at the right hand edge of the pore, i.e. on the side of the pore having the greater separation between the pore and mirror boundaries. Using the pore size as a sharp flaw and the failure stress of 18.5×10^3 psi (128 MPa) gives a γ_p of $\sim 27\,J\,m^2$ which in turn gives $\sigma_p/\sigma_a = 2.6$. M/R for the right hand side of the mirror is 3.1.

locations on opposite sides of the pore, most likely from chips or cracks at pore–tensile-surface intersections. Wallner-line observations (Fig. 8) also support separate failure initiation and outward crack propagation from each pore–tensile-surface intersection when fracture tails are present. Such separate fracture initiation is also consistent with the mirror asymmetry, i.e. the larger pore–mirror boundary distances being on the opposite side of the pore from the tail, since that is the side of the pore from which failure first initiated. This implies that the fracture thus progressed further outward from, and around, the pore before meeting the other crack initiating from the side of the pore on which the tail was located (e.g. Fig. 8). Extreme mirror asymmetries in the absence of fracture tails represent cases in which failure initiated from only one side of the pore. Wallner-line observations (Fig. 9) confirm this and again show failure simultaneously spreading both outward and around the pore. However, growth around the pore typically lagged substantially behind outward growth, producing extremely anisotropic mirrors (e.g. Fig. 9).

The above observations clearly show that failure from one or two areas around a pore is the dominant mode of failure. The occurrence of fracture tails, mirror asymmetry, or both, in the absence of any obvious chips (e.g. Fig. 7),

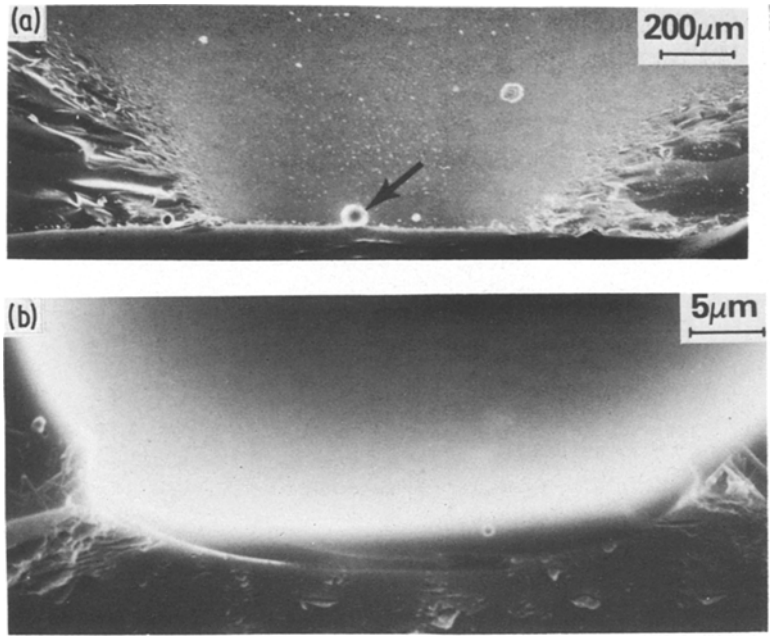

Figure 7 Failure from a pore just opening onto the surface of a soda–lime glass specimen (pore shown by arrow in (a)). In (b) the intersection of the pore with the surface is shown at much higher magnification. Note the relatively symmetrical mirror with $M/R = 8.6$. The failure stress of 15.1×10^3 psi (104 MPa) gives $\gamma_p \sim 6.1\ J\,m^{-2}$ (using the pore as a sharp flaw which in turn gives a σ_p/σ_a value of 1.2.

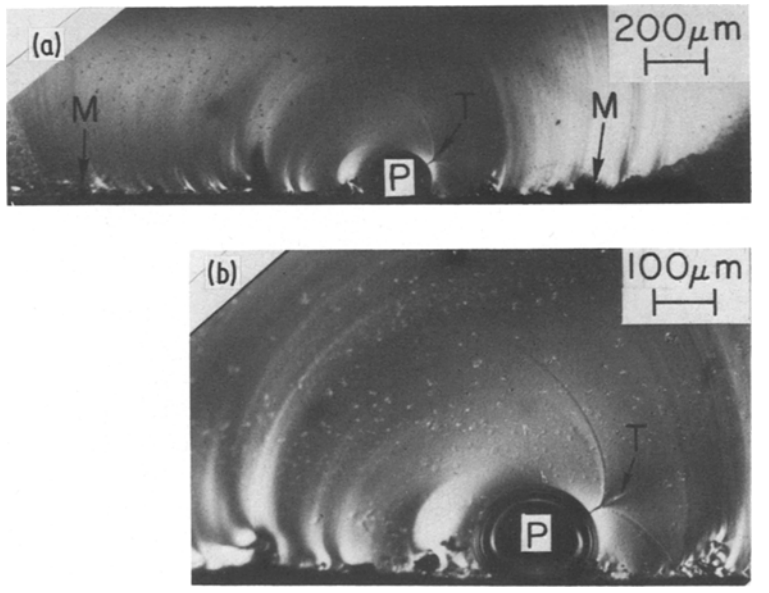

Figure 8 Optical photomicrograph of a large void at the surface. Note in particular the fracture tail, T, (arrow) extending at approximately two o'clock from the pore, P. (a) and (b) Optical photomicrographs showing the actual fracture markings. (c) A sketch of the pore, P, approximate crack-front positions, and resultant fracture tail, T. The 11.7×10^3 psi (81 MPa) failure stress gives a $\gamma_p \sim 8.4\ J\,m^{-2}$ and a resultant $\sigma_p/\sigma_a = 1.4$.

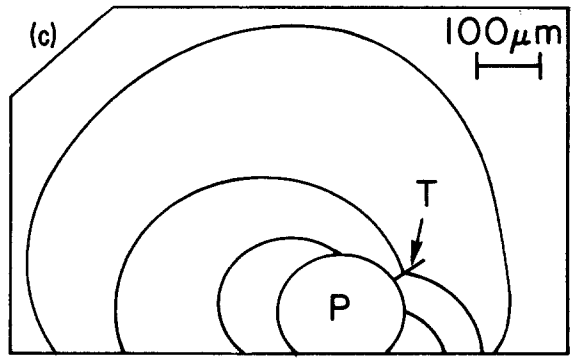

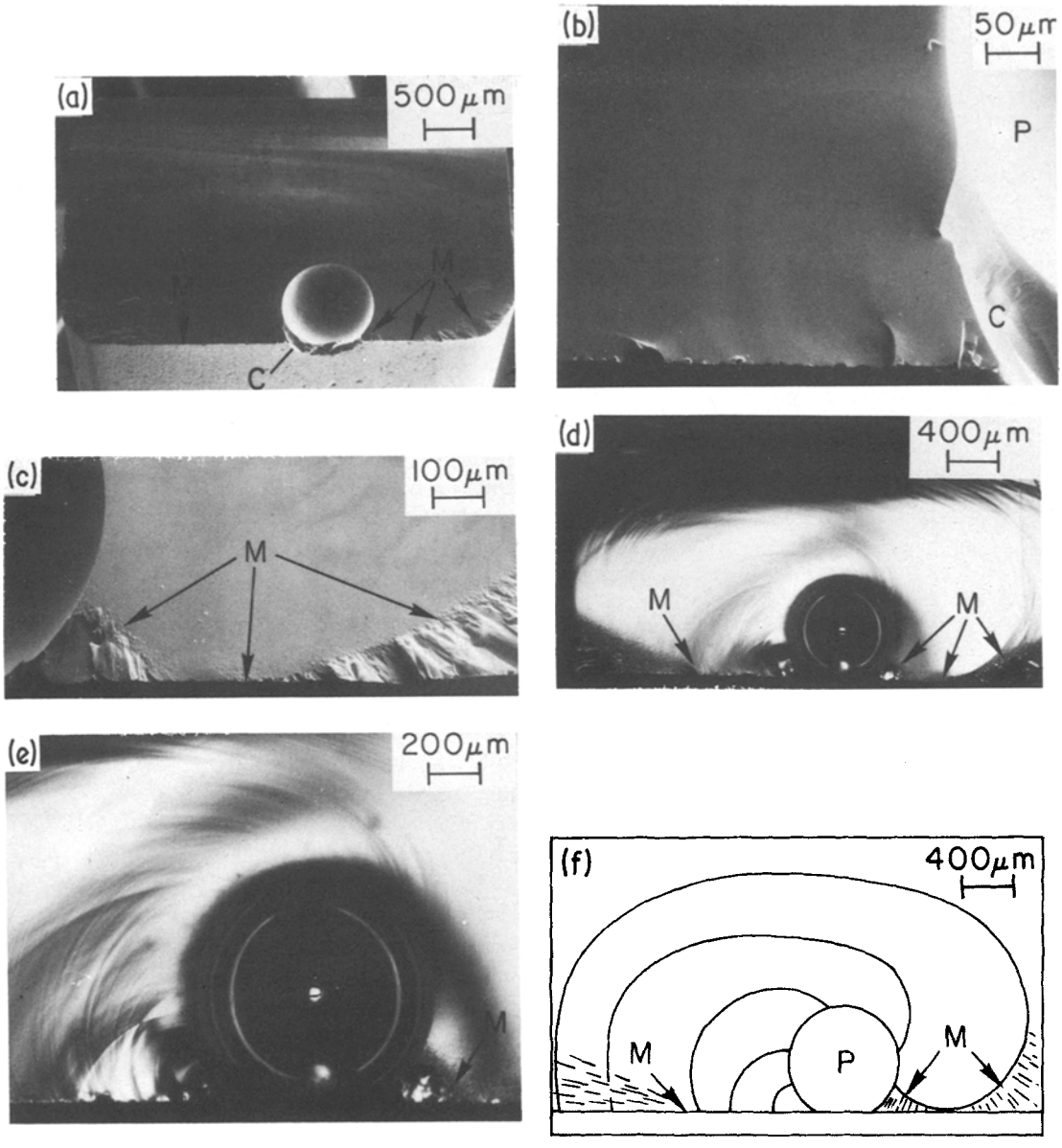

Figure 9 Failure of a soda–lime glass specimen failing from a large pore, P exposed at the surface. (a) to (c) are SEM photographs and (d) and (e) are optical photomicrographs of the matching half of the fracture surface (so the optical reversal gives the same orientation as the SEM photographs), showing much more clearly the fracture markings from which the sequence of failure was sketched in (f). Note the chip, C, on the left edge of the pore at the tensile surface and the great asymmetry of the mirror with the mist and hackle on right edge of the pore pointing upwards, not radially oriented with the pore. The failure stress of 7.65×10^3 psi (53 MPa) gives $\gamma_p \sim 18\ J\,m^{-2}$ and a resultant $\sigma_p/\sigma_a \sim 2.1$. Note the extremely low M/R value of 2.7 using the larger, i.e. left hand dimension of the mirror.

and especially in the case of the internal origin (Fig. 10), where no machining flaws could be present, shows that even subtle variations result in failure initiation along part of the pore periphery, instead of from the complete periphery. Such failure initiation is inconsistent with Evans's evaluation that a partial equatorial crack spreads to a full equatorial crack, then causes failure. Whether this is due to stress gradients in flexure, since Evans's evaluation was in uniform tension, is unknown. In any event, the present flexural results are thus also inconsistent with the equatorial crack assumed in Baratta's, Evans's and Green's models. However, the following analysis shows that despite this difference, their models are at least approximately applicable, and hence

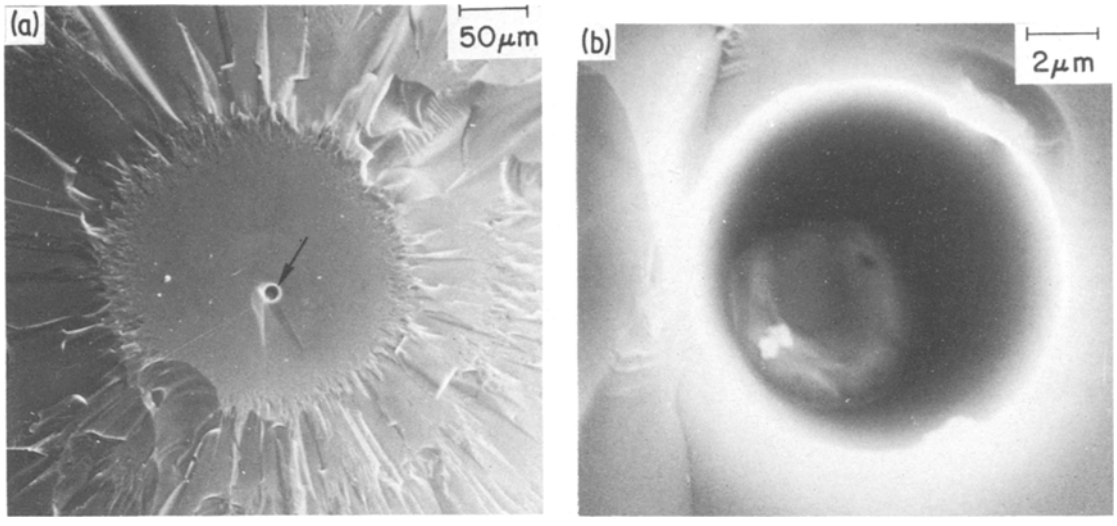

Figure 10 Failure of a flame-polished SiO_2 rod from an internal bubble (arrow in (a)). The bubble (pore) is shown at higher magnification in (b). Note the fracture tail extending down from the bottom portion of the pore in (a). The fracture stress of 76×10^3 psi (520 MPa) (corrected to $\sim 60 \times 10^3$ psi (~ 410 MPa)) at the pore centre gives $\gamma_p \sim 5.5$ J m^{-2}, which in turn gives $\sigma_p/\sigma_a \sim 8.8$. Note that there is some anisotropy to the mirror, giving an M/R of 14 to 18. This anisotropy is believed to be due to the stress gradient in the specimen, which in turn would indicate that the void was not at the maximum-stress (i.e. six o'clock) position relative to the loading axes.

a useful step in the direction of treating pores as fracture origins.

Exact tests of the models cannot be made from the glass results since the exact size and shape of the chips and cracks associated with pores generally could not be determined. Even if they were, the models would not allow for quantitative evaluation for a partial equatorial crack. However, the chips and cracks whose size was consistent with typical machining flaw sizes [1] (see also Figs. 4 and 5) were small in comparison with the pores and on only a small fraction of the periphery, so the pore radius R will be used as the total flaw size. γ_p values (calculated using $E = 70$ GPa) are shown in Table I, along with resultant σ_p/σ_a ratios using $\gamma_a = 4$ J m^{-2}.* The lower bounds for σ_p/σ_a from failures from flaws near voids vary from > 1.1 to > 3.3 (Figs. 3 to 5), and hence in the same range as those of Table I. The calculated σ_p/σ_a values generally correspond to L/R values from the models (Fig. 2) of $\leqslant 0.05$, and often $\leqslant 0.01$. Such values are generally consistent with the crack or chip sizes, or their average over the pore periphery.

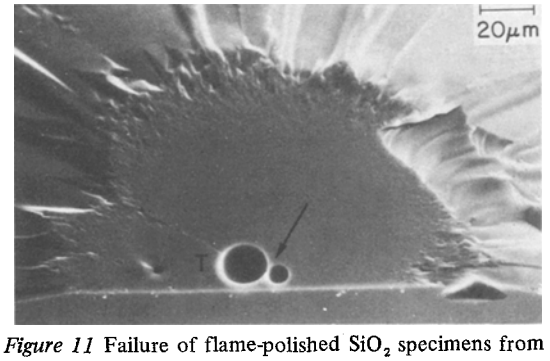

Figure 11 Failure of flame-polished SiO_2 specimens from two touching pores. Note the fracture tails, T, extending from the pores at approximately the 10 o'clock position, and the significant perturbation of the mirror boundary approximately in line with the fracture tail. Failure stress = 74×10^3 psi (510 MPa).

Quantitative analysis of mirror dimensions also supports the above analysis as follows. The failure stress, σ_f, is related to the flaw size, a, and mirror size, M, by the following equation:

$$\sigma_f = \frac{A}{a^{1/2}} = \frac{B}{M^{1/2}} \qquad (2)$$

where A and B are constants for a given material (with sharp flaws), so the ratio of mirror size to flaw size is $M/a = (B/A)^2$. From Equation 1, A is $Z(E\gamma_a)^{1/2}$ for failure from a sharp flaw, but must be multiplied by σ_p/σ_a for failure from a pore.

*Fracture energies calculated from the limited number of flaw origins in this study corroborated $\gamma \sim 4$ J m^{-2} for silica-based glasses. For the germanate glass γ was also found to be ~ 4 J m^{-2} (DCB measurements courtesy of K. McKinney).

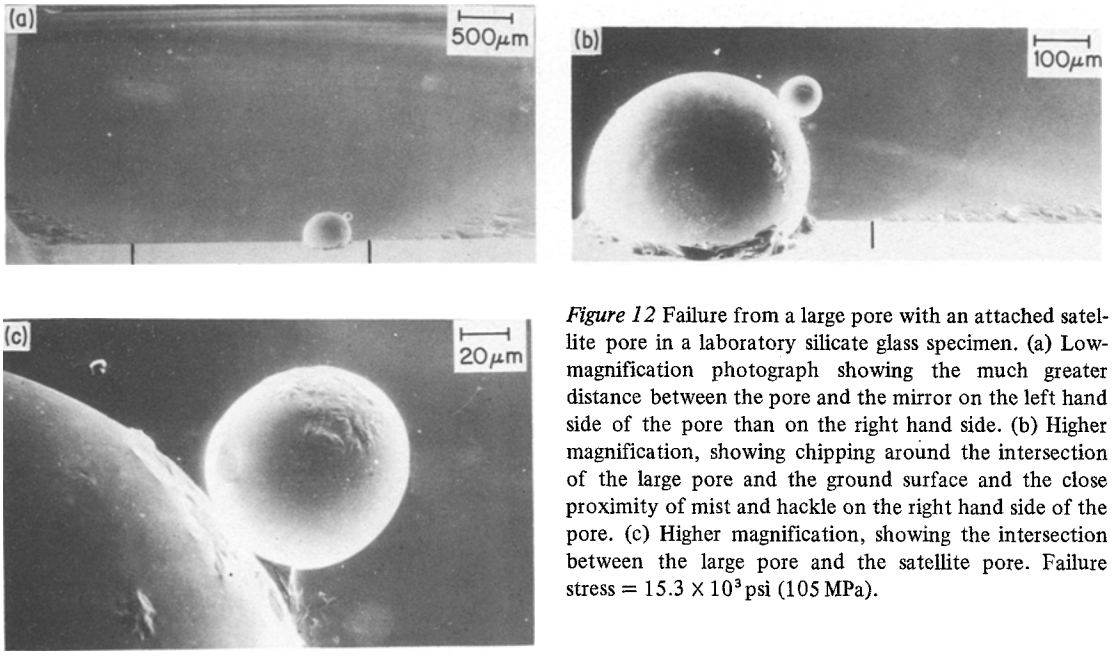

Figure 12 Failure from a large pore with an attached satellite pore in a laboratory silicate glass specimen. (a) Low-magnification photograph showing the much greater distance between the pore and the mirror on the left hand side of the pore than on the right hand side. (b) Higher magnification, showing chipping around the intersection of the large pore and the ground surface and the close proximity of mist and hackle on the right hand side of the pore. (c) Higher magnification, showing the intersection between the large pore and the satellite pore. Failure stress = 15.3×10^3 psi (105 MPa).

The formation of the mirror is by a sharp crack, so B does not involve σ_p/σ_a). Thus, for failure from a pore,

$$M/a = \left(\frac{B}{A}\right)^2 \left(\frac{\sigma_p}{\sigma_a}\right)^{-2} \quad (3)$$

i.e. M/a for failure from a pore is reduced by $(\sigma_p/\sigma_a)^2$, from the value for a sharp flaw, or alternatively M/a for failure from a pore should be multiplied by $(\sigma_p/\sigma_a)^2$ to give the M/a value for failure from a sharp flaw. Multiplying the observed M/a ratios by the observed $(\sigma_p/\sigma_a)^2$ values (Table I) gives reasonable agreement with M/a values for failure from sharp flaws (~ 14). Note that for quite asymmetric mirrors this agreement results only for the larger mirror dimension. This is in agreement with results of Freiman *et al.* [27] who frequently observed asymmetric mirrors around failure from flaws not normal to the stress axis, and that the larger portion of the mirror was always the one agreeing with or approaching the value for symmetrical mirrors.

3.1.3. Analysis of origins from two or more pores

Fracture origins from two or more pores were generally similar to those from single pores, but with some important differences in degree. Thus, fracture tails on one (e.g. Fig. 11) or more (e.g. Fig. 13) of the pores were found, but mirror asymmetry was generally quite limited. Only when one pore was clearly dominant was there considerable asymmetry (e.g. Fig. 12).

Results of calculating γ_p and resultant σ_p/σ_a values, by taking the flaw size as the pore group envelope, the circular flaw of the same cross-sectional areas as the pores, or individual pore sizes, which as noted earlier should bound most, or all, possibilities, are given in Table I. These results raise serious questions about the present concept of closely spaced pores simply linking together to form a larger flaw. If a group of pores were linked together by intervening cracks, then that combination should more closely approach the behaviour of a sharp crack than a single pore. Thus, substantial σ_p/σ_a values, e.g. $\geqslant 2.4$, using either the envelope or the area of the pores as the flaw size, would appear to be inconsistent with the concept of simple linkage by intervening cracks. In these cases, failure might be explained by treating an individual pore as the origin. However, where the cluster envelope or pore area approached sharp flaws, of $\sigma_p/\sigma_a < 1.5$, individual pores gave $\sigma_p/\sigma_a < 1$, an unrealistic value. Thus, there was no consistent behaviour of pore groups, which questions a single, simple model.

The mirror observations from failures with two or more pores also argue against the simple linkage of closely spaced pores by cracks to form a single large flaw. As noted above, such a resultant combined flaw should more closely approach the

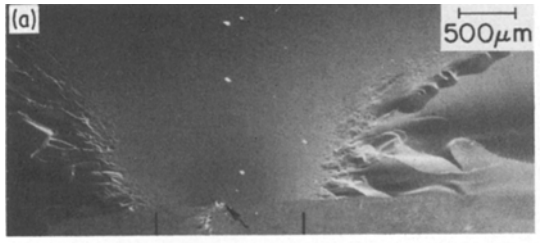

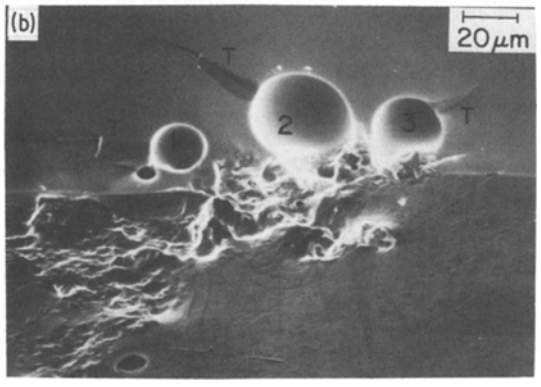

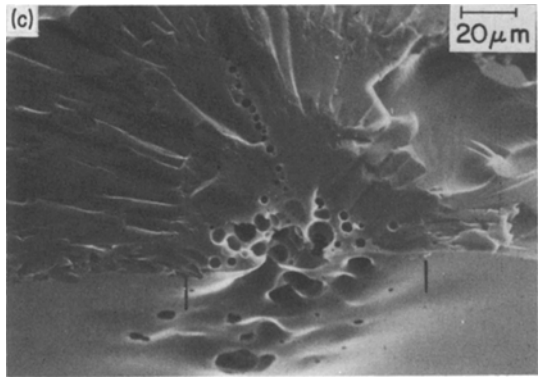

Figure 13 Examples of failures from multiple voids. (a) and (b) SEM photographs of the fracture origin in a laboratory silicate glass specimen failing from a cluster of voids (arrow in (a)) with a relatively symmetrical mirror. (b) Higher magnification, showing that there are three larger voids exposed on the fracture surface, and some associated chipping, particularly around the centre, larger void (number 2). Failure stress = 13.3×10^3 psi (92 MPa). (c) Fracture of a flame-polished SiO_2 specimen with a number of voids in the area of failure initiation and a relatively symmetrical mirror (indicated by vertical lines). Failure stress = 94.9×10^3 psi (654 MPa).

behaviour of a sharp crack than that of a single pore. However, treating the envelope of the pore groups as the flaw size leads to very small M/a ratios, except for one case where one of two pores is much larger than the other so there is not much difference between cases A to C (Table I). Multiplying these values by $(\sigma_p/\sigma_a)^2$ generally gives very high values. On the other hand, analyses based on failure from only one of the pores, or on the equivalent area, result in (M/a) values much closer to the expected M/a value of ~ 14 than does treating the envelope as the flaw. This again questions the consistency of a single model, and especially questions the pore-envelope model.

Another factor arguing against simple pore linkage as the only failure mechanism is the behaviour of the specimen shown in Fig. 12, where failure occurred from a large pore with a satellite pore slightly intersecting the large pore. If simple pore-linking were the typical operative mechanism, one would expect the wedge-shaped webs of material on either side of where the two pores join to have readily fracture, and thus have been points of failure initiation. However, the high anisotropy of the mirror and the fact that the largest pore–mirror distance is on the opposite side of the large pore from the location of the satellite pore show failure initiated from the side of the large pore opposite the satellite pore, so the intersection of the two pores cannot be the origin.

That linkage of pores could be a complicated and variable process can be seen by considering variation in pore perfection, crack propagation around a pore, and especially spatial distribution of pores. As discussed earlier, variations in pore perfection ranging from associated chips or cracks to minor variations in surface topography can significantly effect the initiation of fracture from a pore. Deviations in overall pore shape from the idealized spherical shape should have similar effects. Also, as discussed and demonstrated earlier, cracks almost never stay on the same plane in propagating around a pore, and hence leave fracture tails. Combining these factors with variable spatial distribution can lead to many different possibilities; e.g. consider one pore from which fracture starts and one or more other nearby pores. Thus, for example, even with three pores, whose centres will always be coplanar, the angle of the plane of their centres relative to the loading axis and their features effecting crack initiation and propagation cover a wide range. With more than three pores, two or more non-coplanar cracks

might form, in varying combinations and varying interactions with one another. Thus, normal analysis based on a single, simple crack may often be an inadequate approximation.

Two aspects of the observations of fracture origins with multiple pores corroborate the above analysis of fracture from single pores. First, the variability of pore groups, from behaving as a flaw whose size is the envelope of the group, to the possibility of a single pore of the cluster being the origin, is consistent with the substantial variability seen with single pores. Thus, for example, variable location and severity of defects such as machining flaws may lead to significant variability of failure from a pore cluster. Second, treatment of failure from some of the pore groups as failure from a single pore in that group is equally or more consistent with the results in some cases, and consistent with results obtained for single-pore origins.

3.2. Polycrystalline specimens

3.2.1. Strength and fracture

Results of tests of lead-zirconate-titanate specimens with purposely introduced spherical pores are shown in Table II. Fracture origins were typically from such pores at or very near the tensile surfaces, e.g. Figs. 14 to 16. Since the pores were commonly somewhat clustered, more than one pore was often at, or in the vicinity of, the fracture origin. While it was clear that fractures

TABLE II Analysis of failure from spherical pores in lead zirconate titanate

Spec. No.	Failure stress, σ_f (10^3 psi)	Failure stress, σ_f (MPa)	E (GPa)	Origin		a (μm)	$(Z)^2$	γ_p (J m^{-2})
1B	6.37	44	35	cluster of 4 pores at corner	envelope	225	0.9	11.50
					equiv. area	150	0.9	7.67
				1 pore at corner		100	0.0	5.11
1C	7.81	54	49	cluster of 6 pores at corner	envelope	250	1.5	22.9
					equiv. area	85	0.9	4.67
				1 pore at corner		50	0.9	2.74
1D	7.19	50	49	cluster of 2½ pores at corner	envelope	150	1.4	10.9
					equiv. area	150	0.9	6.98
				1 pore near corner		100	0.9	4.65
3B	6.89	48	49	machining flaw + 3 pores,	envelope	120	0.8	4.56
				1 + 3 pores,	equiv. area	88	0.8	3.34
4B	8.38	58	63	3–4 corner pores, envelope		50	1.5	4.10
4C	9.78	68	63	pores at corner	envelope	100	1.2	8.93
					equiv. area	100	0.9	6.70
					smaller cluster	75	0.9	5.00
4D (see Fig. 16)	10.9	75	63	cluster 4 pores	envelope	80	0.8	5.92
					equiv. area	50	0.8	3.70
				1 pore		30	0.8	2.22
5D	14.6	100	70	1 pore, flaw		10	1.3	1.94
						< 50	0.8	< 7.48
8A	8.93	62	63	2 pores at side	envelope	50	1.7	5.27
	(8.8)	61						(5.12)
	8.93	62	63		1 pore	50	1.3	4.03
								(3.92)
8B (see Fig. 14)	8.88	61	63	1 + 2 half-pores at surface	envelope	175	0.8	8.59
					equiv. area	125	0.8	6.13
					1 pore	100	0.8	4.91
8C (see Fig. 16)	8.40	58	63	4 pores near corner	envelope	350	0.9	17.29
					equiv. area	200	0.9	9.88
					1 pore	70	0.9	3.46
8D	10.1	70	63	1½ pores	envelope	80	1.3	8.25
					equiv. area	90	0.8	5.71
					½ pore	60	0.8	3.81

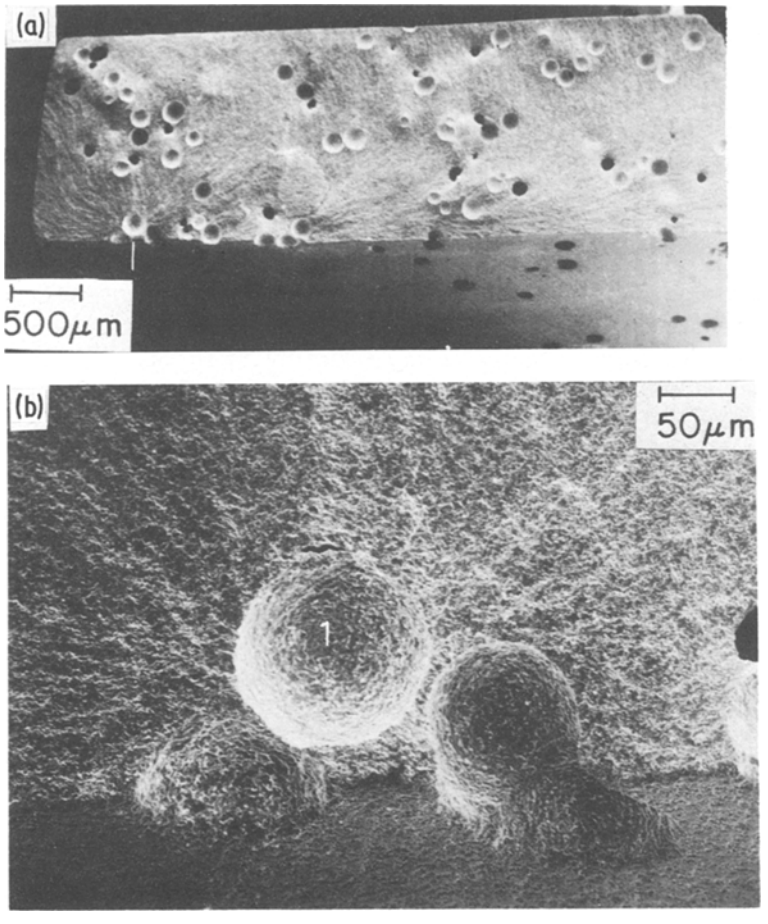

Figure 14 Failure of lead-zirconate-titanate sample with large spherical voids. (a) shows the complete fracture surface. Note the substantial void clustering. The fracture origin is near the left hand side of the specimen from the void group immediately above the vertical white mark. (b) Higher magnification of this fracture area. Note that the fracture markings radiate predominantly from the large central void number 1.

originated from some or all of the pores in the clusters in the vicinity of the origin, which portion of the cluster was the origin generally could not be unequivocably determined from the fracture markings. No cases of failure from flaws with pores nearby were found. Fracture mirrors were generally not clear on these samples, e.g. due to the low strength and small specimen size. Three fracture origins, from machining flaws only, in specimens with little or no porosity were also

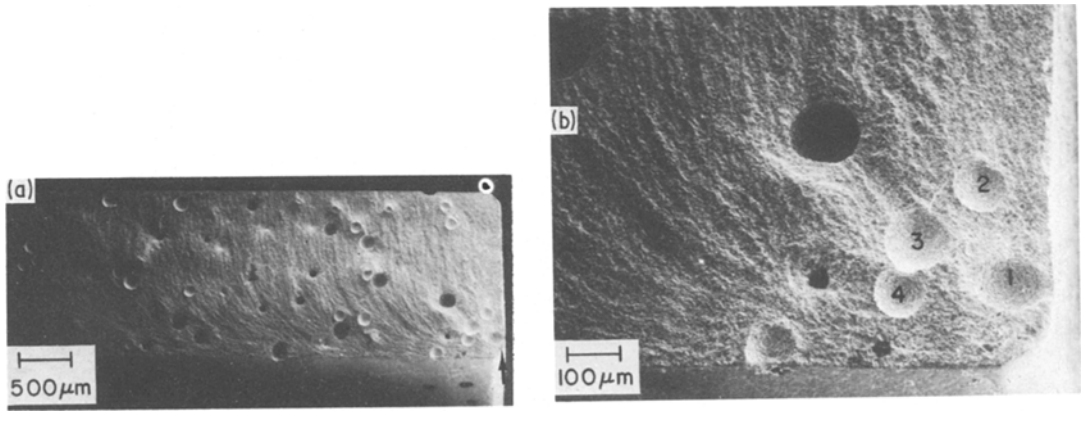

Figure 15 Fracture of lead-zirconate-titranate sample with larger voids near a corner. (a) Low-magnification photo of the specimen. Again note the void clustering. In this case, the fracture origin is near the right hand corner (arrow). (b) Higher magnification of this sample. Note that the fracture evaluation (Table II) indicates that the single pore (1) closest to the surface was the probable failure source, as might be expected because of its greater separation from the other three pores (2, 3 and 4).

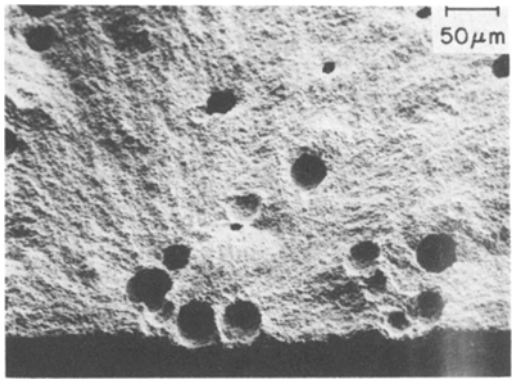

Figure 16 Fracture of lead-zirconate-titanate sample from intermediate-size spherical voids. Note the cluster of four voids at the fracture origin (bottom centre). Evaluation (Table II) indicates that the central single pore give a fracture energy lower than expected fro a probable origin, but that the cluster envelope and the equivalent area of the four pores bracket the expected fracture energy, with either flaw estimate giving a reasonable fracture energy.

found. Fracture energies calculated from these flaws gave results ranging from 4 to 7 $J m^{-2}$ in agreement with literature values of $5 \pm 1 J m^{-2}$ [23].

Data for other polycrystalline samples from other studies are summarized in Table III. Fracture initiation from individual pores was very common; no cases were observed of specimens failing from flaws smaller than pores located where the pores could cause failure. In other words, if individual pores, similar to or larger than other flaws (e.g. machining flaws), were in the region of significant stress then they were the source of failure. In fact, pores considerably inside the tensile surface, e.g. with lower stress on them than on somewhat smaller surface flaws, were frequent sources of failure. Fracture mirrors were typically observed around fracture origins in most of the materials of Table III. These mirrors generally had much less anisotropy in comparison with many of the mirrors on glass fractures originating from individual pores, and were also similar in size to fracture mirrors on specimens of the same materials that failed from flaws of the same size as the pores.

3.2.2. Analysis of origins in lead zirconate titanate with spherical pores

Since two or more pores were typically at the origin due to pore clustering, the same three evaluations noted earlier were used; namely pore envelope, pore area and individual pores as flaw sizes. From Fig. 2, and the concept that pores plus $\sim G/2$ ($\sim 2 \mu m$, Fig. 1) are the flaw sizes for single pores, one would expect σ_p/σ_a values of ~ 1 to 2, and hence γ_p/γ_a values of ~ 1 to 1.4. For multiple pores, these ratios should be much closer to 1 since pores linked by cracks should be still closer to typical sharp-crack behaviour.

Comparison of calculated γ_p values (Table II) with $\gamma_a = \sim 5 J m^{-2}$ from the literature (and limited flaw origins found in this study) show poor agreement using pore-cluster envelopes. Out of the twelve cases, the envelope size gave γ_p values reasponably close to γ_a in only three. In these three cases either there was a significant machining flaw associated with the pores or the pore density was so high that the difference in the envelope flaw size and pore equivalent area was not significant, e.g. within 20%. In about half of the cases γ_p values calculated from the equivalent areas of the pores in the cluster or from the single pore closest to the surface were about equally close to the expected fracture energy (e.g. Fig. 14). The equivalent area flaw generally gave γ_p values within about 1 $J m^{-2}$ higher than 5 $J m^{-2}$ and the single pore flaw generally gave γ_p values within about 1 $J m^{-2}$ lower than 5 $J m^{-2}$. For one case, the equivalent area was closer to the expected value than the single pore. In two cases, the single pore was closer than the equivalent area flaw (e.g. Fig. 15).

The above experimental results and analysis lead to three conclusions. First, since pores were extremely common fracture origins in porous bodies and probable cases of failure from single pores give $\gamma_p \sim \gamma_a$, pores in these bodies acted much more like sharp flaws than they did in glasses or than as predicted by application of the present models (e.g. Fig. 2). Second, since pore envelopes typically did not give reasonable γ_p values, the concept of simple pore-linking as the dominant mechanism of failure from pore groups is further questioned. Third, that there is frequent clustering of these pores and that some fracture origins are clearly from two or more clustered or intersecting pores invalidates modelling of the strength dependence of these bodies based on failure from a single pore [17].

3.2.3. Analysis of typical polycrystalline pores as fracture origins

Calculations in which pores were approximated as spheres of radius R having the same cross-sectional

TABLE III Evaluation of natural pores as fracture origins in polycrystalline ceramics

Failure stress*		Origin†	R‡	γ_p	$L/R = G/2R$	σ_p/σ_a	L§ for $\sigma_p/\sigma_a \sim 1$
(10^3 psi)	(MPa)		(μm)	(J m^{-2})			(μm)
(a) Fine grain ($G \sim 0.5\ \mu$m), PSZ, $ZrO^2 - 6$ w/o Y_2O_3, $\gamma_a = 60 \pm 10$ J m^{-2} ¶							
102	700	I	49	75	0.005	2.7	2.5
96	660	I	50	69	0.005	2.7	2.5
105	724	I	60	74	0.004	3.9	3.0
148	1020	S	11	44	0.045	1.07	0.6
71	490	S	33	31	0.015	1.6	1.7
84	580	S	55	71	0.004	2.9	2.8
92	630	S	60	93	0.004	2.9	3.0
113	7780	S	113	70	0.002	4.1	5.7
(b) Reaction-sintered Si_3N_4 (% porosity given in parentheses), $G \sim 1\ \mu$m**							
35 (16)	240	S	40	10	0.013	1.7	2.0
46 (26)	320	I	32	5	0.016	1.6	1.6
(c) Commercial lead zirconate titanate, $G \sim 5\ \mu$m, $\gamma_a = 5 \pm 1$ J m^{-2} ¶							
9.0	62	I	80	2.4	0.03	1.2	4.0
9.0	62	I	135	4.1	0.02	1.4	6.8
10.4	72	S	35	1.9	0.07	1.0	1.8
11.6	80	S	49	3.9	0.05	1.1	2.5
8.8	61	S	50	1.8	0.05	1.1	2.5
11.0	76	S	87	4.7	0.03	1.2	4.4
6.5	45	S	200	3.9	0.01	1.9	1.0
(d) Hot-pressed Al_2O_3, $G \sim 2\ \mu$m, $\gamma_a = 14 \pm 6$ J m^{-2} ¶							
28.7	198	I	32	1.6	0.03	1.2	1.6
42.8	295	I	34	4.9	0.03	1.2	1.7
30.3	209	I	37	3.3	0.03	1.2	1.8
35.7	246	I	43	5.3	0.02	1.4	2.2
26.4	187	I	45	2.9	0.02	1.4	2.3
26.3	181	I	80	4.9	0.01	1.9	4.0
28.0	193	I	81	6.0	0.01	1.9	4.0
25.8	178	I	94	5.5	0.01	1.9	4.8
16.6	114	I	222	3.9	0.005	2.7	11.1
16.6	114	I	235	4.9	0.004	2.9	11.8
28.7	198	S	37	4.6	0.03	1.2	1.6
35.7	246	S	43	9.7	0.02	1.4	2.3
28.0	193	S	81	9.5	0.01	1.9	4.0
27.0	186	S	125	10.0	0.01	1.9	6.3

*Flexure tests for all materials, except for true tensile tests hot-pressed Al_2O_3.
†S = flaw at surface, I = internal flaw.
‡Radius of equivalent spherical pore.
§L taken as $0.05R$, i.e. where $\sigma_p/\sigma_a < 1.1$.
¶See ref. 23 for more details.
**See ref. 31 for more details.

area of the pore and using $R + G/2$ as the size of sharp flaws for pore origins in various ceramic bodies from past studies [1, 7, 8, 23] gave γ_p* values (Table III) that agreed with values calculated from machining-flaw origins [23]. If the pore models of Baratta, Evans and Green were applied then the γ_p values would have to be divided by the square of the σ_p/σ_a values, using $L = G/2$. This would on the average reduce the calculated fracture energies several fold, giving ridiculously low values. Allowing for some variation in L, e.g. taking $L = G$ instead of $G/2$ in these models, would

*Note that the γ_p values in Table III decrease with decreasing flaw size (i.e. R value), just as the fracture energies for flaw sizes did [23]. This is attributed to increasing effects of internal stresses occurring as the flaw size decreased for the partially stabilized zirconia bodies. This decrease of calculated fracture energy begins below flaw size of 60 to 70 μm, while in the lead zirconate titanate the decrease begins at flaw sizes of slightly over 60 μm and in the Al_2O_3 bodies the decrease begins at flaw sizes of ~ 125 μm. Above these flaw sizes γ values calculated from the flaw size agreed well with those independently measured by fracture-mechanics (e.g. by double cantilever beam) techniques.

not begin to bring reasonable agreement between measured fracture energies and values calculated using resultsnt σ_p/σ_a values. Similarly, Heinrich and Munz [28] have recently reported good agreement between measured and calculated results using $R + G$ as the size of a sharp flaw for failure of reaction-sintered Si_3N_4 (RSSN) from pores (artificially introduced) that acted as a surface origin.

The above evaluation is primarily for pores intersecting the surface; although evaluation of the data in Table III shows no obvious distinction between internal and surface pores, the number of internal pores was quite limited. Further, several of the internal pores were close enough to the surfaces to possibly act as surface pores, e.g. due to connection to the surface by machining flaws. Behaviour of internal pores similar to that of the equivalent sharp flaws is also, at first, suggested by the fractographic data of Suzuki and Hayashi on WC bonded with 10% Co. Over most of the range of their fracture data, i.e. up to a flaw size of 25 to 30 μm, failures from pores show the same strength as failures from WC grains or cobalt agglomerates of the same size. However, at flaw sizes $\geqslant 30$ to 35 μm, their limited data begins to show higher failure stresses (e.g. $\sim 20\%$ for flaw sizes $> 70\,\mu$m) for failure from pores than for WC grains or cobalt agglomerates. These (mainly internal) pore origins show higher σ_p/σ_a values than surface pores, i.e. $\sigma_p/\sigma_a \sim 1.2$ for $a > 70\,\mu$m). Such σ_p/σ_a values are close to, but below, $\sigma_p/\sigma_a >$ 1.6 from Fig. 2. General agreement of failure from pores and sharp flaws at smaller pore sizes is expected from $G \sim 1.7\,\mu$m, giving R/L sufficiently high to approach sharp-flaw behaviour. The limited data of Richerson and cplleagues [29] for reaction-sintered Si_3N_4 (RSSN) with nearly spherical pores ($R \sim 50$ to $100\,\mu$m, $G \sim 1\,\mu$m) show that the behaviour of surface pores is close to, or equal to, that of sharp flaws, but suggests that internal pores may not act so much like sharp flaws as do pores exposed on the surface of test specimens. However, there is insufficient data to quantitatively evaluate possible differences.

Thus, results for crystalline bodies clearly show that pores intersecting, or very near, the tensile surface act very like sharp flaws, i.e. γ_p/γ_a and $\sigma_p/\sigma_a \sim 1$, and hence are often lower than predicted by the models. This similarity between surface pores and sharp flaws is also corroborated by the similarity in mirror size and symmetry for the two types of surface origins. The behaviour of internal pores in polycrystalline bodies may, at least in some cases, be intermediate betweeen that of surface pores and that predicted by models of Baratta, Evans and Green. However, the lack of distinct differences in mirror sizes between internal and surface pore origins indicates that differences, if any, in these two types of pore origins are limited. Machining flaws associated with surface pores are a likely explanation for at least part of their acting as sharp flaws and possibly being more severe than internal pores. However, in glasses with surface pores and associated flaws σ_p/σ_a values were often > 1.

3.2.4. Rationalization of single pore-flaw models with polycrystalline behaviour

There is thus a major question of why pores in polycrystalline bodies appear to behave more like sharp flaws than in glasses. There is also the question, noted in the Introduction, of why failure immediately around such pores is often transrather than intergranular.

Three factors provide a reasonable rationale for the differences indicated between polycrystalline results and glass results and the models. First, the rougher surface topography of polycrystalline pores, due for example to common grain-boundary grooving, provides a rationale for the greater severity of pores as flaws in polycrystalline bodies in view of the sensitivity to pore topography indicated for glasses. Second, application of the near-surface mismatch-stress analysis of Wachtman and Dunduras [30] suggests easier initiation and possibly propagation of flaws at and near the pore surface. They showed that stresses, due to mismatch strains between grains from thermal-expansion anisotropy in the grains, are highly accentuated at, and near, a free surface. As summarized in Fig. 17, such stress accentuation increases up to fivefold as the depth of the grain below the surface decreases (i.e. as G decreases). Such local increases would appear to be a likely reason why pores in fine-grain polycrystalline bodies act more as sharp flaws, since the finer the grain size,* the greater the accentuation. Since the stress accentuation is

*For fine grains around a pore, the stress accentuation can extend more than one grain deep, so resultant cracks may be a few grains in extent, e.g. L ~ 1G to 3G. However, this will typically not cause significant errors since in such cases, $G \ll R$, so R is still the dominant factor in the flaw size.

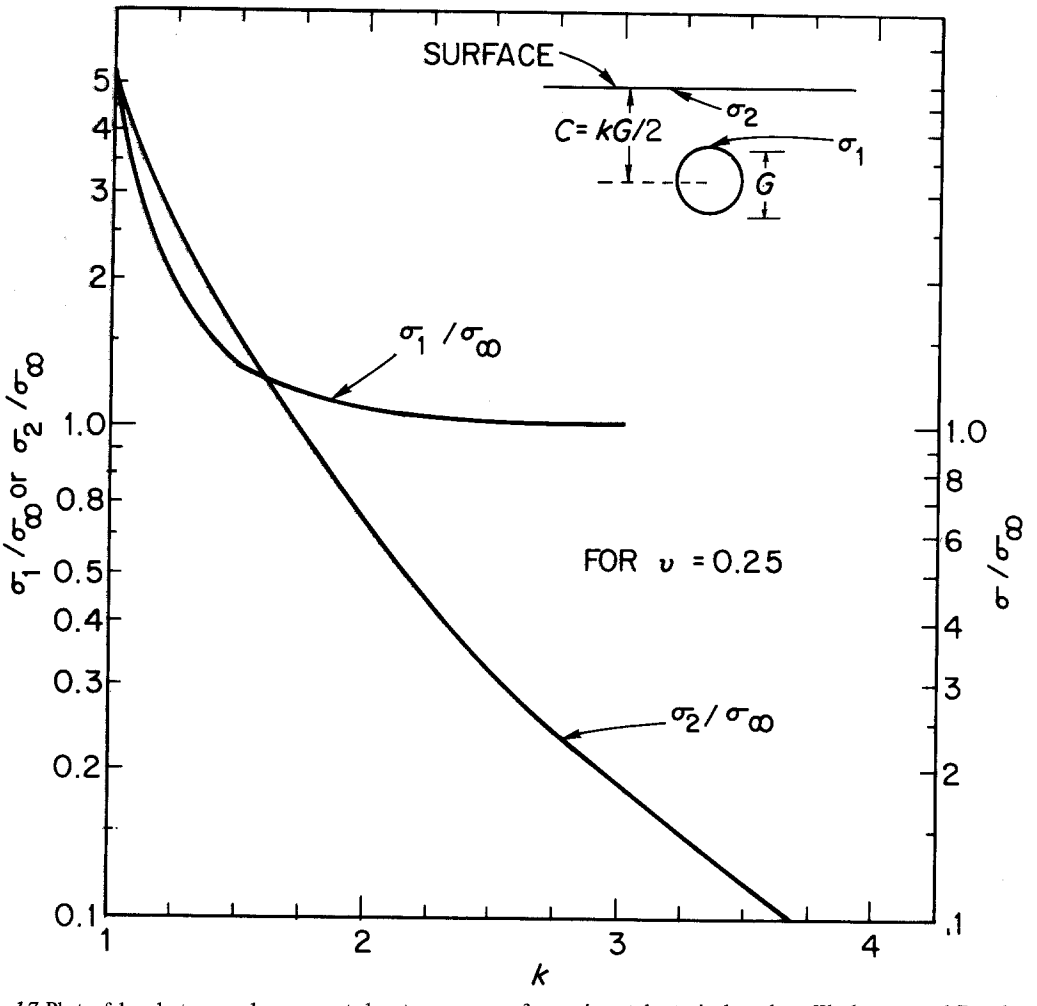

Figure 17 Plot of local stress enhancement due to a near-surface mismatch strain based on Wachtman and Dunduras's analysis. σ_1 is the stress at the surface of a (spherical) grain (diameter G), σ_2 the stress at the surface (in this case the pore surface) directly above the grain centre, and σ_∞ is the value of σ_1, when $C \to \infty$; i.e. when the grain is far below the surface. Thus $\sigma_1/\sigma_\infty \to 1$ and $\sigma_2/\sigma_\infty \to 0$ for large C, and hence large k as shown.

similar to σ_p/σ_a values found in glasses, the two would approximately cancel. On the other hand, as G increases, the stress accentuation decreases, but so does σ_p/σ_a, so again, an approximate cancellation would be expected. Wachtman and Dunduras treated only thermal-expansion anisotropy, i.e. for bodies of noncubic crystal structures or two-phase character. However, similar mismatch strains and associated stresses occur owing to elastic anisotropy, and hence in all polycrystalline bodies when under an applied load, i.e. when tested to failure.

The third factor providing a rationale for the difference between polycrystalline results and the models is the relation of L and G. While the concept of $L \sim G/2$ (or $\sim G$; this difference is normally insignificant) has a possible physical basis, there is no demonstration that this is correct, as Baratta [32] has pointed out. Thus, for example, such a fixed relation between L and G neglects the stress-concentration effect of the pore. This depends on both the distance from the pore surface, r, and the pore radius, R, i.e. it goes as $(R/r)^3$. Thus, the distance from a pore for a given level of stress concentration varies linearly with the pore size. Results for calculating L to make $\sigma_p/\sigma_a \sim 1$ for the polycrystalline results, i.e. at $L/R \sim 0.05$, shown in Table III simply give L as $\sim 0.05R$, and hence increasing linearly with pore size. This gives L starting at $\sim G/2$ to G, and increasing to a few times G as R increases, as does similar evaluation of Heinrich and Munz's RSSN data. This is physically quite realistic, i.e. L starting at $\sim G/2$ to G for small pores, but increasing,

quite possibly approximately as multiples of $G/2$ or G, as R increases. These increases in L are small in comparison to the total flaw size. Thus, increasing L with R generally causes negligible increases in the flaw size and hence negligible change in treating the pore- $+\sim G$ as a sharp flaw, while bringing the pore-flaw model into agreement with the results.

The frequent trans- instead of only intergranular fracture around pores is felt to be rationalized by fracture energy-geometry and stress considerations. If a crack forming around a void is only a few grains in extent due to large grain or small void size, or if it forms in small steps of a grain or so at a time, then intergranular fracture could reflect lower fracture energies, i.e. grain boundary versus single-crystal fracture energies. However, the geometry of the intergranular path reflects greater fracture-surface area (Fig. 1b) and associated Mode II and III fracture that can compensate for possible lower grain-boundary fracture energies. Further, while the transgranular path may possibly be deeper (i.e. greater L) than an intergranular path (Fig. 1), such greater depth is still commonly within the significant stress-concentration range of the pore, and such greater crack-depth significantly reduces σ_p/σ_a (Fig. 2) and hence the failure stress, thus significantly favouring the deeper crack. The stress accentuation of Wachtman and Dunduras may also be a factor since it depends on the misorientations between the grains, so there will be a wide statistical variation in stresses between grains and especially along various triple lines. Thus, some deeper triple lines may have greater stress accentuation than some shallower ones (i.e. those labelled **b** against those labelled **a** in Fig. 1a. These factors, combined with the complex nature of such stress, may often favour transgranular fracture.

4. Summary and conclusions

Individual pores in glasses are generally less severe sources of failure than sharp flaws of the same dimensions. Qualitatively, this is consistent with the pore models of Baratta, Evans and Green. However, considerable variability occurs, especially for surface pores, where variable, but poorly delineated, chipping and cracking from machining appear to be important. Detailed fractographic studies show that pores with an associated crack do not form an equatorial crack as an intermediate stage of failure. Such studies also show that the "blunter" the pore is as a fracture origin, the smaller the ratio of the mirror size to pore (flaw) size (M/a). However, multiplying M/a by $(\sigma_p/\sigma_a)^2$ corrects for these low values.

Individual pores in polycrystalline bodies, especially pores at or intersecting the surface, behave much more like sharp flaws than do pores in glasses. This is generally consistent with the concept of sharp flaws forming into the surrounding grains. Such cracks appear to start from a limit of approximately one grain deep around small pores, but as pore size increases crack depth may well increase, possibly as multiples of $G/2$ or G. Since often $G \ll R$, such increases in radial crack size, L, generally do not negate the use of $R + G$ as the approximate size of a sharp flaw. Probable reasons for the frequent trans- instead of only intergranular fracture around pores at fracture origins in polycrystalline bodies are also given.

The concept of closely spaced pores, e.g. with centre-to-centre separations of $\leqslant 4R$, readily linking to form a larger flaw was found too often not be valid in glasses or polycrystalline specimens. Analysis indicates that such linking is substantially less common than previously predicted, and may be quite variable, e.g. sensitive to local chipping and cracking from machining, as well as to pore positions and resultant possible secondary, e.g. microcrack, flaw formation. Such variations pose a substantial challenge for quantitative nondestructive evaluation (NDE).

Acknowledgement

The author gratefully acknowledges significant aid of Mr A. Gonzales in preparing and testing specimens and Mrs Morey in SEM photography as well as Dr A. Evans for earlier discussions of pore failure, and Drs D. Lewis and F. Baratta for discussion of the manuscript.

References

1. R. W. RICE, "Treatise on Materials Science and Technology", Vol. 11, edited by R. K. McCrone, (Academic Press, 1977) p. 199.
2. A. G. EVANS and R. W. DAVIDGE, *J. Nucl. Mater.* **33** (1969) 249.
3. A. G. EVANS and R. W. DAVIDGE, *J. Mater. Sci.* **5** (1970) 314.
4. J. R. McLAREN, G. TAPPIN and R. W. DAVIDGE, *Proc. Brit. Ceram. Soc.* **20** (June, 1972) 259.
5. A G. EVANS and G. TAPPIN, *Proc. Brit. Ceram. Soc.* **20** (June 1972) 275.
6. O. L. BOWIE, *J. Mater. Phys.* **35**(1) (1956) 60.
7. B. MOLNAR and R. W. RICE, *Am. Ceram. Soc.*

Bull. **52**(6) (1973) 505.
8. R. W. RICE, "Fracture Mechanics of Ceramics", Vol. 1, edited by R. C. Bradt, D. P. H. Hasselman and F. F. Lange, Plenum Press, New York, 1974) p. 323.
9. F. I. BARATTA, *J. Am. Ceram. Soc.*, **61** (11–12) (1978) 490.
10. *Idem, ibid.* **62** (9–10) (1979) 528.
11. *Idem,* "Refinement of Stress Intensity Factors for a Peripherally Cracked Spherical Void and a Hemispherical Surface Pit–Revisited" (Army Materials and Mechanics Research Center, Watertwon, MA 02172, submitted to *J. Am. Ceram. Soc.*).
12. A. G. EVANS, D. R. BISWAS and R. M. FULRATH, *J. Am. Ceram. Soc.* **62**(1–2) (1979) 101.
13. D. J. GREEN, *J. Amer. Ceram. Soc.* **63** (5–6) (1980) 342.
14. R. W. RICE and J. J. MECHOLSKY, Jr, "The Science of Ceramic Machining and Surface Finishing", Vol. II, edited by B. J. Hockey and R. W. Rice (*National Bureau of Standards Special Publication 562,* Oct. 1979), p. 351.
15. D. R. BISWAS, University of Microfilms Int. (Ann Arbor, Mich.) Order No. 77-15,902; *Diss. Abstr. Int. B.* **38**(2) (1977) 842.
16. D. R. BISWAS and R. M. FUBRATH, "Fracture Mechanics of Ceramics, edited by R. C. Bradt, D. P. H. Hasselman and F. F. Lange (Plenum Press, 1978) p. 933.
17. O. VARDAR, I. FINNIE, D. R. BISWAS and R. M. FULRATH, *National J. Fract.* **13**(2) (1977) 215.
18. R. W. RICE, "Surfaces and Interfaces of Glass and Ceramics", edited by V. D. Frechette, W. C. LaCourse and V. L. Burdick (Plenum Press, New York, 1974) p. 439.
19. J. J. MECHOLSKY, R. W. RICE and S. W. FRIEMAN, *J. Am. Ceram. Soc.* **57** (1974) 440.
20. J. J. MECHOLSKY, S. W. FRIEMAN and R. W. RICE, *J. Mater. Sci.* **11** (1976) 1310.
21. J. J. MECHOLSKY, Sandia Lab., private communication (1979).
22. J. J. MECHOLSKY, S. W. FRIEMAN and S. M. MOREY, Naval Research Laboratory Interim Technical Report 1, Prepared for Defense Advanced Research Projects Agency ARPA Order No. 3285 (1977).
23. R. W. RICK, R. C. POHANKA and W. J. McDONOUGH, *J. Am. Ceram. Soc.*, accepted for publiction.
24. H. SUSUKI and K. HAYASKI, "Planseeberickte für Pulvermetallurgie", Bd. 23 (1975) p. 24.
25. G. R. IRWIN and P. C. PARIS, "Fracture, An Advanced Treatise", Vol. 3, edited by H. Liebowitz (Academic Press, 1971), p. 2.
26. G. K. BANSAL, *J. Amer. Ceram. Soc.* **59** (1976) 1.
27. S. W. FRIEMAN, A. C. GONZALES and J. J. MECHOLSKY, *J. Am. Ceram. Soc.* **62** (1979) 3.
28. J. HEINRICK and D. MUNZ, *Amer. Ceram. Soc. Bull.*, accepted for publication.
29. D. W. RICHERSON, Technical Report 21-2794(08) for Air Force Wright Aeronautical Labs., Materials Lab. and Aero-Propulsion Lab., Feb. (1980) p. 105.
30. J. B. WACHTMAN, Jr, and J. DUNDURAS, *Amer. Ceram. Soc.* **54**(10) (1971).
31. R. W. RICE, S. W. FREIMAN and J. J. MECHOLSKY, Jr, "Ceramics for High Performance Applications" edited by J. J. Burke, E. N. Lenoe and R. N. Katz (Brook Hill Pub. Co., Chestnut Hill, Mass., 1978) p. 669.
32. F. I. BARATTA, *Comm. Am. Ceram. Soc.* C-32-C-34 (1981).

Received 15 February
and accepted 21 July 1983